Wireless Optogenetics

Jordan G. McCall, MPH, Tae-il Kim, PhD, Gunchul Shin, PhD, Yei Hwan Jung, Xian Huang, PhD, Fiorenzo G. Omenetto, PhD, John A. Rogers, PhD, and Michael R. Bruchas, PhD

Department of Materials Engineering, University of Illinois
Urbana-Champaign, Illinois
Departments of Anesthesiology and Neurobiology
Washington University in St. Louis
St. Louis, Missouri

NOTES

Introduction

In neuroscience generally, and in optogenetics in particular, an ability to insert light sources, detectors, sensors, and other components into precise locations of the deep brain could yield versatile and important capabilities. Here, we introduce an injectable class of cellular-scale optoelectronics that offers such features, with examples of unmatched operational modes in optogenetics. These include completely wireless and programmed behavioral control over freely moving animals.

Electronic systems that integrate with the body provide powerful diagnostic and therapeutic capabilities for basic research and clinical medicine. Recent research establishes materials and mechanical constructs for electronic circuits, light emitting diodes (LEDs), sensors, and other components that can wrap the soft, external surfaces of the brain, skin, and heart for diverse function in analytical measurement, stimulation, and intervention (Sekitani et al., 2009; Qing et al., 2010; Tian et al., 2010; Viventi et al., 2010; Kim et al., 2010, 2011). A significant constraint in operating these devices, however, follows from their surface-mounted configurations and inability to provide direct interaction into the volumetric depths of tissues. Passive penetrating electrodes or optical fibers with interconnections to externally located electronic control/acquisition systems or light sources can be valuable in many contexts—particularly in neuroscience, engineering, and surgery (Anikeeva et al., 2012; Mattis et al., 2012; Stark et al., 2012). Direct biological integration is limited by challenges from tissue lesions during insertion, persistent irritation, and engineering difficulties in thermal management, encapsulation, scalable interconnection, power delivery, and external control. Many of these issues constrain attempts to insert conventional bulk LEDs into brain tissue (Kim et al., 2012b) and to use semiconductor nanowire devices as cellular probes or active, *in vitro* tissue scaffolds (Tian et al., 2010, 2012).

In optogenetics, engineering limitations of conventional, tethered fiber optic devices restrict opportunities for *in vivo* use and widespread biological application. As a solution, we developed mechanically compliant, ultrathin multifunctional optoelectronic systems that mount on releasable injection needles for insertion into the depth of soft tissue. These wireless devices incorporate cellular-scale components ranging from independently addressable, multicolored microscale inorganic light-emitting diodes (μ-ILEDs) to colocated, precision optical, thermal, and electrophysiological sensors and actuators.

Design and Function of Wireless Optoelectronics

Figure 1*A* presents a scanning electron micrograph (SEM) of an isolated gallium nitride (GaN) μ-ILED, as a constituent component of these systems, and an epifluorescent image of a device among cultured HEK293 cells to illustrate the similar sizes. Each such "cellular-scale" μ-ILED (6.45 μm thick, 50 × 50 μm^2) uses high-quality epitaxial material grown on sapphire, processed to establish contacts (15 × 15 μm^2 square pads in the corners, and an L-shaped current-spreading layer for the p-contact) and then released, to allow transfer printing onto narrow, thin plastic strips. The μ-ILEDs are more than 1,000 times smaller than conventional LEDs (typically 100 μm thick, with lateral dimensions of 1 mm^2) and fiber optic probes (Kim et al., 2012b). The small sizes of μ-ILEDs allow for spatially precise, cellular-scale delivery of photons, highly effective thermal management, limited power requirements, reduced tissue damage, and minimized inflammation for prolonged use *in vivo*.

Combining μ-ILEDs with electronic sensors and actuators yields multifunctional integrated systems that can be configured in single or multilayer formats. Figures 1*B* and *C* illustrate the latter option. In this format, the sensors/actuators include the following: a microelectrode for electrophysiological recording or electrical stimulation (Layer #1; a 20 × 20 μm^2 exposure defines the active area); a microscale inorganic photodetector (μ-IPD) based on an ultrathin silicon photodiode (Layer #2; 1.25 μm thick, 200 × 200 μm^2); a collection of 4 μ-ILEDs connected in parallel (Layer #3); and a precision temperature microsensor or microheater (Kim et al., 2013). Each layer is processed on separate substrates shaped to match a releasable, photolithographically defined epoxy microneedle. A thin layer (~500 nm) of epoxy joins each layer in a precisely aligned, stacked configuration. The microneedle bonds to the bottom layer with a thin, bioresorbable silk fibroin, enabling removal of the microneedle after implantation (Fig. 1*D*). The temperature sensors determine the degree of local heating, with a precision approaching ~1 mK, and can be used as microheaters. The μ-IPD can measure the intensity of light from the μ-ILEDs while implanted deep in brain tissue and/or enable basic spectroscopic evaluations of absorption, fluorescence, diffuse scattering, etc. (Kim et al., 2013).

NOTES

Implantation and Device Function

Injection of such flexible devices into the brain follows the steps shown in Figure 1*D*. The injected multifunctional optoelectronic systems have a total thickness of ~20 μm. This exceptionally thin geometry, low bending rigidity, and high degree of mechanical flexibility (Figs. 1*E*, *F*) allow for minimally invasive operation. Wired control schemes use standard transistor–transistor logic (TTL) and are therefore compatible with any electrical commutators. Details on wired powering strategies and optogenetic functionality in rodent behavioral assays are presented in Kim et al., 2013.

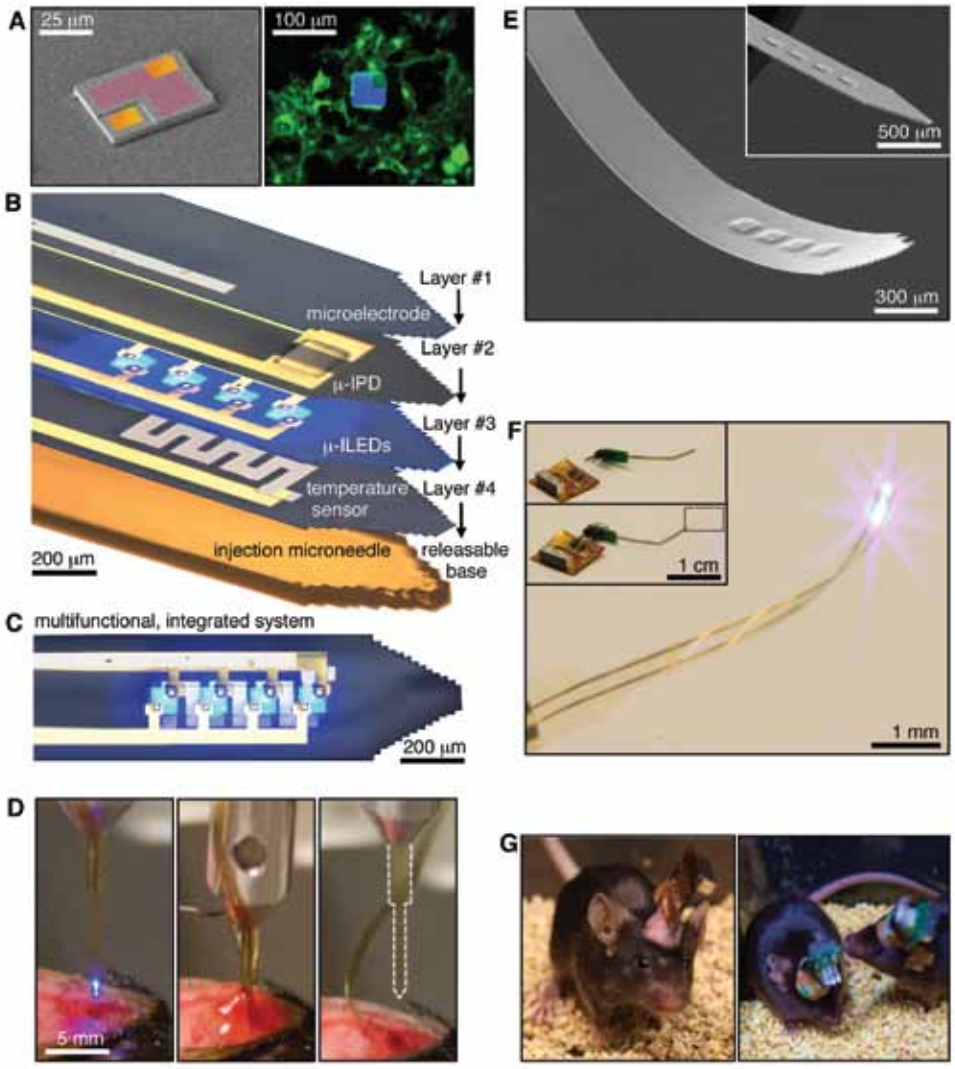

Figure 1. Injectable, cellular-scale semiconductor devices, with multifunctional operation in stimulation, sensing, and actuation. ***A,*** Left, colorized SEM of a GaN μ-ILED (~6.45 μm thick, and 50 × 50 μm^2; contacts: gold; spreading layer: red). Right, fluorescent image of a μ-ILED (blue) with cultured HEK293 cells that express an eYFP-tagged transmembrane protein (green). ***B,*** A multifunctional, implantable optoelectronic device, in a tilted exploded-view layout illustrating various components. The system includes layers for electrophysiological measurement (layer #1; Pt contact pad, microelectrode), optical measurement (layer #2; silicon μ-IPD), optical stimulation (layer #3; μ-ILED array), and temperature sensing (layer #4; serpentine Pt resistor), all bonded to a releasable structural support for injection (microneedle). ***C,*** Top view of the integrated device shown in *B*. ***D,*** Process of injection and release of the microneedle. After insertion, artificial cerebrospinal fluid (center) dissolves the external silk-based adhesive. The microneedle is removed (right), leaving only the active device components in the brain. ***E,*** SEM of an injectable array of μ-ILEDs. The total thickness is 8.5 μm. Inset shows rigid device before coating with a passivation layer. ***F,*** Integrated system wirelessly powered with RF scavenging. Insets show a connectorized device unplugged (top) and plugged into (bottom) the wireless power system. ***G,*** Healthy, freely moving mice with lightweight, flexible (left) and rigid (right) wireless systems powering GaN μ-LED arrays in the VTA. Scale bars: ***A,*** Left, 25 μm; right, 100 μm; ***B,*** 200 μm; ***C,*** 200 μm; ***D,*** 5 mm; ***E,*** 300 μm; inset, 500 μm; ***F,*** 1 mm; insets, 1 cm.

NOTES

Figure 1*F* shows the implementation of a wireless power module based on radiofrequency (RF) scavenging. A custom flexible polyimide film-based lightweight (~0.7 g) power scavenger or a rigid printed circuit board–based scavenger (~2.0 g; Fig. 1G) can be acutely and temporarily mounted on freely moving animals without constraining their natural animal behavior (Fig. 1G). The entire system consists of a wireless power transmitter and RF signal generator; an RF source (910 MHz; power output between 0.02 and 0.1 mW); a power supply; an RF power amplifier (gain of 49 dB at 910 MHz; power output between 1.6 and 7.9 W); and a panel antenna (gain of 13 dBi). The low-frequency signal generator provides user-controlled amplitude modulation for programmed operation. The RF power that reaches the animals, under normal operating conditions at a distance of ~1 m, is between 0.15 and 0.77 mW/cm^2, which is substantially smaller than the maximum permissible exposure (MPE) limits (3.03 mW/cm^2) for humans (FCC). Wireless control allows access to complex and ethologically relevant models in diverse environmental settings, including social interactions, home-cage behaviors, wheel running, complex maze navigation tasks, and many other behavioral outputs (Fig. 1G).

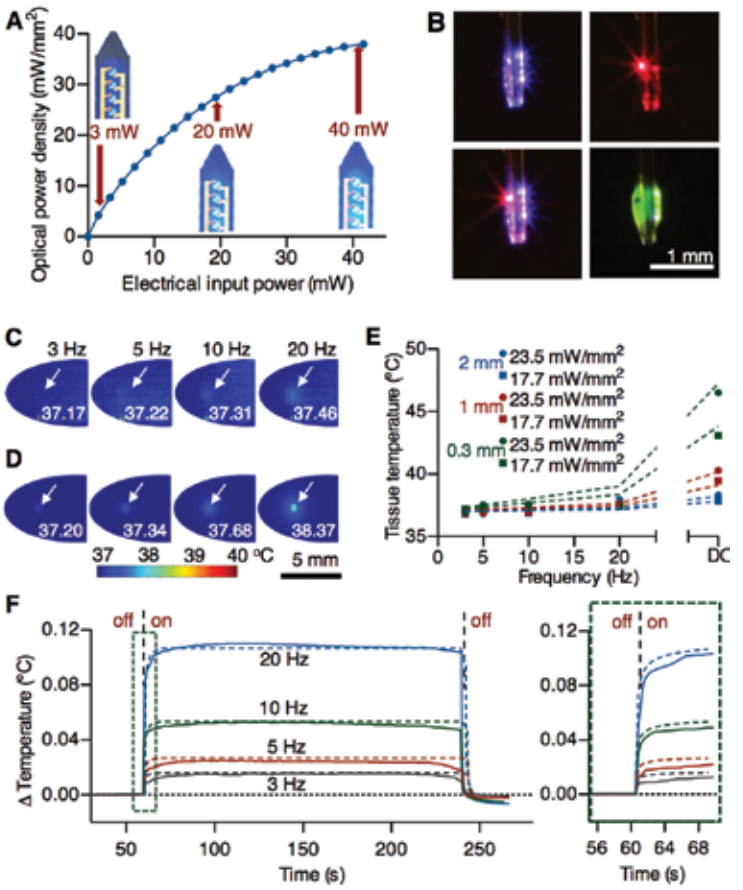

Figure 2. Optical, thermal, and electrophysiological studies with corresponding theoretical analyses. ***A,*** Total optical power density as a function of electrical input power applied to an array of four GaN μ-ILEDs; optical images show operation at 3, 20, and 40 mW. ***B,*** A single device has one 675 nm GaAs μ-ILED and four 450 nm GaN μ-ILEDs that can be activated either independently (top left and top right) or concurrently (bottom left). The same device is coated in a fluorescein sodium salt phosphor for 530 nm light (bottom right). ***C,*** Measured and ***D,*** calculated temperatures in explanted brain tissue near implanted μ-ILEDs at a depth of 0.3 mm and operated at 17.7 mW/mm^2 of light output power. ***E,*** Temperatures in a system similar to that of *C* and *D,* as a function of duty cycle in the operation of the μ-ILEDs and at three different implantation depths (0.3, 1.0, and 2.0 mm) and two different light output powers (17.7 and 23.5 mW/mm^2). ***F,*** Change in brain temperature as a function of time, measured using an integrated temperature sensor colocated with an array of four μ-ILEDs in a lightly anesthetized mouse. Results were evaluated at peak input electrical power of 8.65 mW, in 3, 5, 10, and 20 Hz pulses (10 ms duration). The vertical dashed lines indicate onset (at 60 s) and offset (at 240 s) of the μ-ILEDs. Colored dashed lines correspond to theoretical models for the temperature. The right frame shows the time dynamics as the device is powered. Scale bars: ***B,*** 1 mm; ***C, D,*** 5 mm.

The electrical, optical, and thermal characteristics of the devices when operated in biological environments are important for optogenetics and other biomedical applications. Figure 2A shows the total optical power density of the 4 μ-ILEDs in this device as a function of electrical input power (Kim et al., 2013). This performance is comparable with similarly designed, state-of-the-art conventional GaN LEDs (Kim et al., 2013). Many optogenetic constructs can be activated with ~1 mW/mm^2, at wavelengths near 450 nm (Mattis et al., 2012). These conditions are well matched to the output of the GaN μ-ILEDs. An input power of ~1.0–1.5 mW (Fig. 2A) is sufficient for both activation of the channelrhodopsin-2 (ChR2(H134)) ion channel and precise control of intracellular signaling (cAMP and ERK 1/2) via an optically sensitive G-protein coupled receptor (Optoβ2) (Figs. 3C, *D*, 5) (Airan et al., 2009). Wirelessly, at a distance of 1 m, the RF scavenger outputs 4.08 mW of electrical power, resulting in a 7 mW/mm^2 optical power density.

NOTES

Other wavelengths are possible using different types of μ-ILEDs, either in multicolored or uniform arrays. Figure 2*B* shows an example of the latter, with blue and red gallium arsenide (GaA) μ-ILEDs, and the former, with green devices.

Figures 2C and *D* show μ-ILED–induced changes in temperature determined by infrared imaging and analytical calculation, respectively. The μ-ILEDs were implanted 0.3 mm into an explanted piece of brain tissue held at 37°C. The time-averaged temperatures measured at light-pulse (10 ms) frequencies of 3, 5, 10, and 20 Hz with peak light output of 17.7 mW/mm2 are 37.17°, 37.22°, 37.31°, and 37.46°C, respectively. These results are similar to calculated time-averaged temperatures of 37.20°, 37.34°, 37.68°, and 38.37°C, respectively. The input power used in these tests is 10 times greater than what is necessary to activate many optogenetic constructs (Mattis et al., 2012). The cellular-scale dimensions of the μ-ILEDs enable high rates of thermal spreading, and the brain tissue operates as an efficient heat sink. The latter property is apparent in studies of the dependence of operating temperature on tissue thickness, operating power, and frequency (Fig. 2E). (More details appear in Kim et al., 2013.) Figure 2F shows changes in temperature measured *in vivo* using an integrated temperature sensor compared with calculated results.

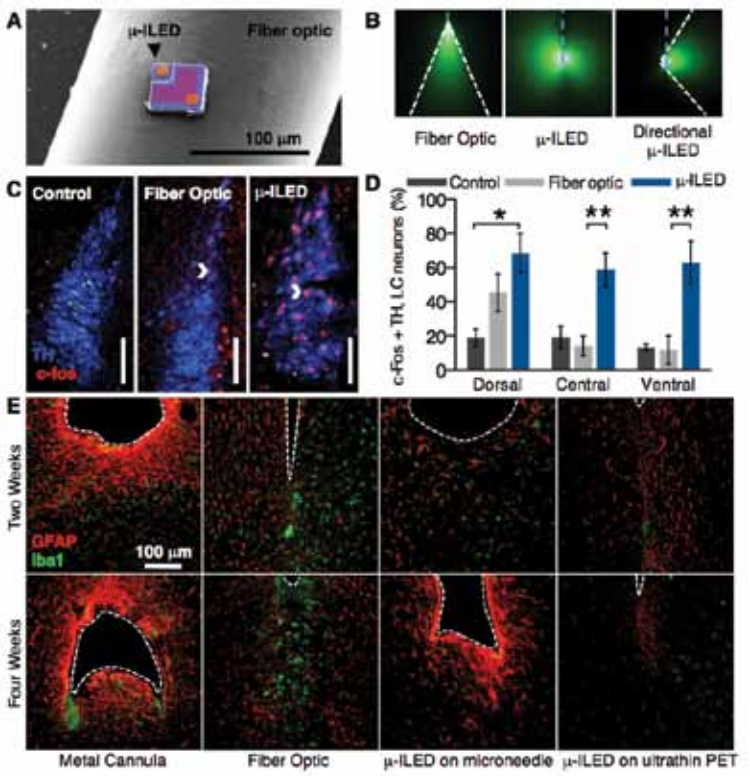

Figure 3. μ-ILED devices improve spatial targeting and reduce gliosis. ***A,*** Colorized SEM (left) of a μ-ILED mounted on a standard 200 μm fiber optic implant. ***B,*** Left, a dorsal-ventral–oriented light cone (outlined in white) from a 200 μm bare fiber implant (blue dashes) emitting 465 nm light in 30 μM fluorescein water. Center, near-omnidirectional light escape from a μ-ILED device (blue dashes) with four 450 nm μ-ILEDs. Right, lateral light escape (outlined in white) from a modified μ-ILED device (blue dashes) to allow unique spatial targeting, including flanking positions along the dorsal-ventral axis of brain loci. ***C,*** Confocal fluorescence images of 30 μm brainstem slices containing the LC show staining for tyrosine hydroxylase (TH, blue) and c-Fos (red) in control (left), fiber optic implanted (center), and μ-ILED device–implanted (right) animals following 1 h, 3 Hz photostimulation (15 ms pulses; 5 mW output power). ***D,*** Fiber optic and μ-ILED treatments specifically increase coimmunoreactivity. Ventral portions of the LC the μ-ILED devices express a higher proportion of tyrosine hydroxylase (TH) and c-Fos coimmunoreactive neurons than fiber optic or control groups (n = 3 slices per brain from 3 brains for each group; two-way ANOVA with Bonferroni's test; all error bars represent means ± SEM; $^{*}p < 0.05$, $^{**}p < 0.01$). ***E,*** Confocal fluorescence images of 30 μm striatal slices show staining for astrocytes (GFAP, red) and activated microglia (Iba1, green) at the ventral tip of each implanted device (dashed outline). Gliosis is smallest with the μ-ILED device at both 2-week and 4-week time points. Scale bars: ***A, C, E,*** 100 μm. PET, positron emission tomography.

Collectively, these results indicate that changes in temperature associated with the operation of μ-ILEDs can be less than 0.10°C for pulse frequencies less than 20 Hz, typical of many neuronal firing rates and lower than those that occur in human deep-brain stimulation (DBS) regulation, ~2°C (Elwassif et al., 2006). In wireless operation, no appreciable change in temperature is associated with operation at the head-stage antenna or skull. To demonstrate functionality of the silicon μ-IPD, Figure 2G shows photocurrents generated by different intensities of light from μ-ILEDs at different pulse frequencies. Finally, the Pt microelectrode has a 400 μm^2 exposure site with ~1.0 MΩ impedance at 1 kHz, capable of measuring extracellular potentials on the μV scale for distinguishing individual action potentials (Figs. 2*H, I*).

In Vivo Operation: Wireless Optical Control of Behavior

For use in optogenetics, such devices eliminate the need for lasers, bulk LEDs, fiber coupling systems, tethers, and

NOTES

optomechanical hardware used in conventional approaches. Absorbing/reflecting structures around the emissive areas of the μ-ILEDs enable precise delivery of light to cellular subregions. Figures 3*A* and *B* compare relative size and the different patterns of light emission from μ-ILEDs with fiber optic probes. Fiber optics typically approach brain structures dorsally. This approach preferentially illuminates cells in the dorsal portion of the targeted region, with greater light intensity near the point of light escape (Fig. 3*B*, left) (Aravanis et al., 2007). Targeting ventral cell bodies or terminals requires lesion of dorsal regions or the use of substantially greater, potentially phototoxic (Yizhar et al., 2011) amounts of light to the site of interest. Neither option protects the intact architecture of a complete brain locus. Though recent advances have spatially restricted light from implanted fiber optics (Tye et al., 2011; Zorzos et al., 2012), these approaches require invasive metal cannulae (Fig. 3*E*) or rely on sophisticated and sensitive engineering that may limit their use in awake, behaving animals. The architecture of the μ-ILEDs enables light delivery medial or lateral to the intended target brain region. Native light escape from μ-ILEDs is nearly omnidirectional (Fig. 3*B*, center) but can be restricted to a wide range of angles with absorbing or reflective structures on the device (Fig. 3*B*, right).

We acutely implanted both μ-ILEDs and fiber optics into animals expressing ChR2(H134)-eYFP in the locus ceruleus (LC). One hour of output-matched photostimulation induced c-fos expression, a biochemical marker of neuronal activation, in both groups of ChR2(H134)-eYFP–expressing mice that was not seen in green fluorescent protein (GFP)–expressing controls (Figs. 3*C, D*). The spatial distribution of c-Fos expression, however, differed markedly between the fiber optic and μ-ILED groups. μ-ILED devices produced significantly greater activation in the ventral LC (Fig. 3*D*).

The physical sizes and mechanical properties of the μ-ILED systems reduce lesioning, neuronal loss, gliosis, and immunoreactivity. Glial responses are biphasic, with an early phase featuring widespread activation of astrocytes and microglia, and a late, prolonged phase hallmarked by restriction

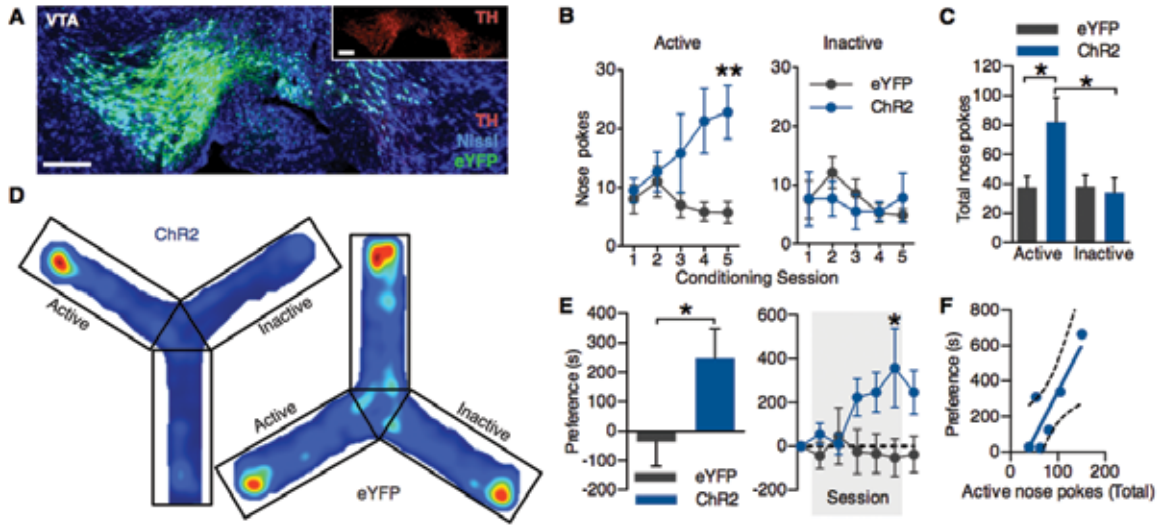

Figure 4. Wirelessly powered μ-ILED devices operantly drive-conditioned place preference. ***A,*** Cell type–specific expression of ChR2(H134)-eYFP (green) in dopaminergic, TH (red)–containing neurons of the VTA. For clarity, inset shows TH channel alone. All scale bars = 100 μm. ***B,*** Operant learning curve on the active (left) and inactive (right) nose poke devices over 5 days of 1 h trials in the Y-maze. Active pokes drive 1 s of 20 Hz light (5 ms pulses) from the μ-ILED device on a fixed-ratio-1 schedule (n = 6–8 mice/group; two-way ANOVA with Bonferroni's test; $^{**}p < 0.01$). ***C,*** Mean number of nose pokes ± SEM across all 5 conditioning sessions. ($^{*}p < 0.05$; one-way ANOVA with Bonferroni's test). ***D,*** Heat maps of activity during the posttest; hotter colors represent longer duration in a location in that part of the apparatus. ***E,*** Left, place preference scores calculated as posttest minus pretest in the active nose poke–paired context. Five days of self-stimulation significantly conditioned a place preference that developed over the course of the training sessions and remained during the posttest (right; $^{*}p < 0.05$ t test compared with controls; $^{*}p < 0.05$ two-way ANOVA with Bonferroni's test). All error bars represent means ± SEM. ***F,*** Scatter plot demonstrating positive correlation ($r = 0.8620$; $p = 0.0272$) between posttest preference and total number of active nose pokes during training in the ChR2(H134)-eYFP group.

NOTES

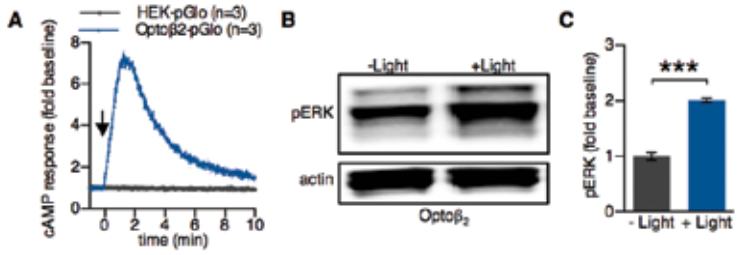

Figure 5. μ-ILED–induced activation of cAMP and ERK phosphorylation in Optoβ2-expressing cells. ***A***, Optoβ2 cells coexpressing pGlo show a rapid and transient increase in cAMP following light (450 nm, 5 s, 0.5 W/cm^2 pulse) stimulation ($n = 3$). HEK293 cells expressing pGlo show no response to the same light stimulation ($n = 3$). Data are expressed as mean ± SEM. ***B***, Representative pERK and actin Western blots for Optoβ2 and HEK293 cells following light (450 nm, 1 min, 0.5 W/cm^2 pulse) stimulation ($n = 3$). ***C***, Quantitation of pERK normalized to actin in light-stimulated Optoβ2 and HEK293 cells (*$p < 0.05$; unpaired, two-tailed *t* test).

of the gliosis to the area closest to the implanted substrate (Szarowski et al., 2003). The μ-ILED devices produced substantially less glial activation and caused smaller lesions as compared with metal cannulae and fiber optics, at both early (2 weeks) and late (4 weeks) phases (Fig. 3*E*). Furthermore, the brain tolerates the thin, flexible devices better than rigid structures (Fig. 3*E*), consistent with reports on passive electrode devices (Kozai and Kipke, 2009). Finally, we examined the chronic functionality of the devices and demonstrated that they are well tolerated in freely moving animals with encapsulated sensors and μ-ILEDs, maintaining function over 3–6 months.

We next implemented a fully wireless system for dissecting complex neurobiology and behavior. Phasic neuronal firing of ventral tegmental area–dopaminergic (VTA-DA) neurons encodes salient stimuli and is sufficient for behavioral conditioning (Tsai et al., 2009; Adamantidis et al., 2011; Coque et al., 2011; Kim et al., 2012a). We selectively targeted ChR2(H134)-eYFP to VTA-DA neurons (Fig. 4*A*) and tested whether mice would engage in wireless, optical self-stimulation (5 ms pulses every nose poke) of their dopamine reward pathway. To increase the contextual salience of the stimulation and demonstrate wireless function of the μ-ILED devices, the mice were free to explore a complex environment. In the absence of physical reward, the same stimulation of VTA-DA neurons that drives a traditionally conditioned place preference (Tsai et al., 2009; Adamantidis et al., 2011) is actively sought with a cued nose poke when paired within a discrete environmental context. ChR2(H134)-eYFP mice learned to self-stimulate their dopamine neurons (Figs. 4*B*, *C*) and, furthermore, developed a robust place preference (Figs. 4*D*, *E*) for the environmental context containing the active nose poke for VTA-DA stimulation. ChR2(H134)-eYFP animals showed a strong correlation ($r = 0.8620$; $p = 0.0272$) between the number of active nose pokes and the magnitude of conditioned place preference that was absent in eYFP controls (Fig. 4*F*).

In addition, we examined the effects of wireless tonic stimulation of VTA-DA neurons on anxiety-like behavior. Five hertz tonic stimulation reduced anxiety-like behavior, whereas phasic activation of VTA-DA neurons did not have an effect on anxiety-like behavior. These findings are consistent with the anxiolytic actions of nicotine on VTA-DA neurons as well as the behavioral phenotypes seen in the *Clock*Δ19 mice that have increased tonic firing of VTA-DA neurons (Coque et al., 2011; McGranahan et al., 2011). They further establish the utility of wireless optogenetic control in multiple environmental contexts.

Conclusion

These experiments demonstrate that these wireless devices can be readily used in optogenetic experiments. Future possible uses are in closed-loop operation, where actuators (heat, light, electrical, etc.) operate in tandem with sensors (temperature, light, potential, etc.) for altering light stimulation in response to physiological parameters such as single-unit activity, pH, blood oxygen or glucose levels, and neurochemical changes associated with neurotransmitter release. Many of the attributes that make these devices useful in optogenetics suggest they also have strong potential for broader use in biology and medicine. The demonstrated compatibility of silicon technology in these injectable, cellular-scale platforms foreshadows sophisticated capabilities in electronic processing and biological interfaces. Biocompatible deep-tissue injection of semiconductor devices and integrated systems such as those reported here will accelerate progress in both basic neuroscience and translational technologies.

NOTES

Acknowledgments

This work is supported by the National Institutes of Health Common Fund, the National Institute of Neurological Disorders and Stroke Grant R01NS081707 (M.R.B., J.A.R.), the National Institute on Drug Abuse Grant R00DA025182 (M.R.B.), the McDonnell Center for Systems Neuroscience (M.R.B.), National Security Science and Engineering Faculty Fellowship of Energy (J.A.R.), U.S. Department of Energy, Division of Materials Sciences under Award No. DE-FG02-07ER46471 (J.A.R.), the Materials Research Laboratory and Center for Microanalysis of Materials (DE-FG02-07ER46453) (J.A.R.), and Washington University in St. Louis Division of Biology and Biomedical Sciences (WUSTL DBBS) (J.G.M.). We thank Hu Tao (Tufts University) and Sukwon Hwang (University of Illinois, Urbana-Champaign) for their help in preparing the silk solution. We thank the Bruchas laboratory and Robert W. Gereau, IV (WUSTL) and Garret D. Stuber (University of North Carolina) for helpful discussion. We thank Karl Deisseroth (Stanford University) for the channelrhodopsin-2 (H134) and OPTO-β2 constructs, G. Stuber for the TH-IRES-Cre mice, the WUSTL Bakewell Neuroimaging Laboratory Core, and the WUSTL Hope Center Viral Vector Core. This chapter is a modified version of a previously published article: Kim TI, et al. *Science*. 2013;340:211–216.

References

Adamantidis AR, Tsai H-C, Boutrel B, Zhang F, Stuber GD, Budygin EA, Touriño C, Bonci A, Deisseroth K, De Lecea L (2011) Optogenetic interrogation of dopaminergic modulation of the multiple phases of reward-seeking behavior. J Neurosci 31:10829–10835.

Airan RD, Thompson KR, Fenno LE, Bernstein H, Deisseroth K (2009) Temporally precise *in vivo* control of intracellular signalling. Nature 458:1025–1029.

Anikeeva P, Andalman AS, Witten I, Warden M, Goshen I, Grosenick L, Gunaydin LA, Frank LM, Deisseroth K (2012) Optetrode: a multichannel readout for optogenetic control in freely moving mice. Nat Neurosci 15:163–170.

Aravanis AM, Wang L-P, Zhang F, Meltzer LA, Mogri MZ, Schneider MB, Deisseroth K (2007) An optical neural interface: *in vivo* control of rodent motor cortex with integrated fiberoptic and optogenetic technology. J Neural Eng 4:S143–S156.

Coque L, Mukherjee S, Cao J-L, Spencer S, Marvin M, Falcon E, Sidor MM, Birnbaum SG, Graham A, Neve RL, Gordon E, Ozburn AR, Goldberg MS, Han M-H, Cooper DC, McClung CA (2011) Specific role of VTA dopamine neuronal firing rates and morphology in the reversal of anxiety-related, but not depression-related behavior in the *Clock*Δ19 mouse model of mania. Neuropsychopharmacology 36:1478–1488.

Elwassif MM, Kong Q, Vazquez M, Bikson M (2006) Bio-heat transfer model of deep brain stimulation-induced temperature changes. J Neural Eng 3:306–315.

Kim D-H, Viventi J, Amsden JJ, Xiao J, Vigeland L, Kim Y-S, Blanco JA, Panilaitis B, Frechette ES, Contreras D, Kaplan DL, Omenetto FG, Huang Y, Hwang K-C, Zakin MR, Litt B, Rogers JA (2010) Dissolvable films of silk fibroin for ultrathin conformal bio-integrated electronics. Nat Mater 9:511–517.

Kim D-H, Lu N, Ma R, Kim YS, Kim RH, Wang S, Wu J, Won SM, Tao H, Islam A, Yu KJ, Kim TI, Chowdhury R, Ying M, Xu L, Li M, Chung HJ, Keum H, McCormick M, Liu P, et al. (2011) Epidermal electronics. Science 333:838–843.

Kim KM, Baratta MV, Yang A, Lee D, Boyden ES, Fiorillo CD (2012a) Optogenetic mimicry of the transient activation of dopamine neurons by natural reward is sufficient for operant reinforcement. PLoS One 7:e33612.

Kim TI, Jung YH, Song J, Kim D, Li Y, Kim H, Song I-S, Wierer JJ, Pao HA, Huang Y, Rogers JA (2012b) High-efficiency, microscale GaN light-emitting diodes and their thermal properties on unusual substrates. Small 8:1643–1649.

Kim TI, McCall JG, Jung YH, Huang X, Siuda ER, Li Y, Song J, Song YM, Pao HA, Kim RH, Lu C, Lee SD, Song IS, Shin G, Al-Hasani R, Kim S, Tan MP, Huang Y, Omenetto FG, Rogers JA, et al. (2013) Injectable, cellular-scale optoelectronics with applications for wireless optogenetics. Science 340:211–216.

Kozai TDY, Kipke DR (2009) Insertion shuttle with carboxyl terminated self-assembled monolayer coatings for implanting flexible polymer neural probes in the brain. J Neurosci Methods 184:199–205.

NOTES

Mattis J, Tye KM, Ferenczi EA, Ramakrishnan C, O'Shea DJ, Prakash R, Gunaydin LA, Hyun M, Fenno LE, Gradinaru V, Yizhar O, Deisseroth K (2012) Principles for applying optogenetic tools derived from direct comparative analysis of microbial opsins. Nat Methods 9:159–172.

McGranahan TM, Patzlaff NE, Grady SR, Heinemann SF, Booker TK (2011) α4β2 nicotinic acetylcholine receptors on dopaminergic neurons mediate nicotine reward and anxiety relief. J Neurosci 31:10891–10902.

Qing Q, Pal SK, Tian B, Duan X, Timko BP, Cohen-Karni T, Murthy VN, Lieber CM (2010) Nanowire transistor arrays for mapping neural circuits in acute brain slices. Proc Natl Acad Sci USA 107:1882–1887.

Sekitani T, Yokota T, Zschieschang U, Klauk H, Bauer S, Takeuchi K, Takamiya M, Sakurai T, Someya T (2009) Organic nonvolatile memory transistors for flexible sensor arrays. Science 326:1516–1519.

Stark E, Koos T, Buzsáki G (2012) Diode probes for spatiotemporal optical control of multiple neurons in freely moving animals. J Neurophysiol 108:349–363.

Szarowski DH, Andersen MD, Retterer S, Spence AJ, Isaacson M, Craighead HG, Turner JN, Shain W (2003) Brain responses to micro-machined silicon devices. Brain Res 983:23–35.

Tian B, Cohen-Karni T, Qing Q, Duan X, Xie P, Lieber CM (2010) Three-dimensional, flexible nanoscale field-effect transistors as localized bioprobes. Science 329:830–834.

Tian B, Liu J, Dvir T, Jin L, Tsui JH, Qing Q, Suo Z, Langer R, Kohane DS, Lieber CM (2012) Macroporous nanowire nanoelectronic scaffolds for synthetic tissues. Nat Mater 11:986–994.

Tsai H-C, Zhang F, Adamantidis A, Stuber GD, Bonci A, De Lecea L, Deisseroth K (2009) Phasic firing in dopaminergic neurons is sufficient for behavioral conditioning. Science 324:1080–1084.

Tye KM, Prakash R, Kim S-Y, Fenno LE, Grosenick L, Zarabi H, Thompson KR, Gradinaru V, Ramakrishnan C, Deisseroth K (2011) Amygdala circuitry mediating reversible and bidirectional control of anxiety. Nature 471:358–362.

Viventi J, Kim D-H, Moss JD, Kim Y-S, Blanco JA, Annetta N, Hicks A, Xiao J, Huang Y, Callans DJ, Rogers JA, Litt B (2010) A conformal, bio-interfaced class of silicon electronics for mapping cardiac electrophysiology. Sci Transl Med 2:24ra22.

Yizhar O, Fenno LE, Davidson TJ, Mogri M, Deisseroth K (2011) Optogenetics in neural systems. Neuron 71:9–34.

Zorzos AN, Scholvin J, Boyden ES, Fonstad CG (2012) Three-dimensional multiwaveguide probe array for light delivery to distributed brain circuits. Opt Lett 37:4841–4843.